Article Title Page

[Effect of the graphene on the methyl methacrylate beam under lateral low velocity impact]

Author Details *(please list these in the order they should appear in the published article)*

Author 1 Name: Raed Salman Saeed Alhusseini
Email: raedalhosainy2019@gmail.com
Department: Department of Power Mechanics
University/Institution: Technical Institute of Babylon, Al-Furat Al-Awsat Technical University
Town/City: Najaf
State (US only):
Country: Iraq

Author 2 Name: Ali Sadik Gafer Qanber
Email: alialseide@gmail.com
Department: Department of Power Mechanics
University/Institution: Technical Institute of Babylon, Al-Furat Al-Awsat Technical University
Town/City: Najaf
State (US only):
Country: Iraq

Author 3 Name: Bashar Dheyaa Hussein Al-Kasob
Email: bashar.dheyaa@atu.edu.iq
Department: Department of Power Mechanics
University/Institution: Technical Institute of Babylon, Al-Furat Al-Awsat Technical University
Town/City: Najaf
State (US only):
Country: Iraq

Author 4 Name: Manar Hamid Jasim
Email: manaralhasan2017@gmail.com
Department: Department of Civil Engineering
University/Institution: Technical Institute of Babylon, Al-Furat Al-Awsat Technical University
Town/City: Najaf
State (US only):
Country: Iraq

Author 5 Name: Mehdi Ranjbar
Email: ranjbar.mehdi88@gmail.com
Department: Department of Power Mechanics
University/Institution: Technical Institute of Babylon, Al-Furat Al-Awsat Technical University
Town/City: Najaf
State (US only):
Country: Iraq

NOTE: affiliations should appear as the following: Department (if applicable); Institution; City; State (US only); Country. No further information or detail should be included

Corresponding author: [Mehdi Ranjbar]
Corresponding Author's Email: ranjbar.mehdi88@gmail.com

☐ *Please check this box if you do not wish your email address to be published*

Effect of the graphene on the methyl methacrylate beam under lateral low velocity impact

Journal:	*World Journal of Engineering*
Manuscript ID	Draft
Manuscript Type:	Research Paper
Keywords:	Methyl methacrylate, graphene, cantilever beam, low velocity impact, energy method

Title: Effect of the graphene on the methyl methacrylate beam under lateral low velocity impact

Purpose – This paper presents the potential of using aligned single layer graphene sheets to reinforce the methyl methacrylate cantilever beam in low velocity impact problem.

Design/methodology/approach – The Halpin-Tsai law is applied to compute the mechanical properties of isotropic polymer beam reinforced by aligned graphene sheet. Using both longitudinal and lateral displacements in composite beam, all components of the stress and strain fields are written. The equations of motion are derived by applying energy method, generalized Lagrange equations and Ritz method.

Findings – The analytical formulation accuracy is corroborated by comparing the present results with those available in the literature. Numerical examples indicate that the contact duration is decreased with increasing of graphene volume fraction while the values of peak contact force, shear strain and shear stress at peak contact force tend vice versa. Also, among the results, shear stress at the peak contact force has the most effect with graphene volume fraction changes.

Originality/value – This research fulfils an identified need to investigate how graphene reinforced beam behavior subjected to low velocity impact can be enabled.

Keywords: Methyl methacrylate, graphene, cantilever beam, low velocity impact, energy method.

Article Type: Research paper

1.introduction

An allotrope of carbon is graphene in the form of a single layer of atoms in a two-dimensional hexagonal lattice in which one atom forms each vertex. Compared to other allotropes such as graphite, charcoal, carbon nanotubes and fullerenes, graphene is the basic structural element. Due to its unique optical, electrical and mechanical properties, graphene has attracted a great deal of interest from researchers in recent years (Li and Kaner, 2008, Huang et al., 2012).

In general boundary conditions, Kiani et al. (Kiani et al., 2013) performed a theoretical and numerical procedure to derive response of low velocity impact on the FGM beams. Using theoretical formulation, Jam and Kiani (Jam and Kiani, 2015) carried out analysis about functionally graded carbon nanotube reinforced composite beams under low velocity impact. An experimental study on nanocomposite beams reinforced with nano-clay subjected to low velocity impact is carried out by Heydari-Meybodi et al. (Heydari-Meybodi et al., 2016). Based on the Extended High Order Sandwich Panel Theory, Salami (Salami, 2017) analyzed low velocity impact on the the sandwich beam with carbon nanotube reinforced composite face sheets and soft core. Ranjbar and Feli (Ranjbar and Feli, 2019b, Ranjbar and Feli, 2018, Ranjbar and Feli, 2019a) analytically, numerically and experimentally performed low velocity impact response of beams and micro-beams reinforced by uniform and axially functionally graded carbon nanotubes based on the classical and modified couple stress theory. In order to consider the combined local denting and global deformation, Qin et al.

(Qin et al., 2017) presented a theoretical approach for low velocity impact on the metal foam core sandwich beams. Based on the rigid-plastic material approximation with modifications, low-velocity impact analysis of fully clamped sandwich beams with fiber-metal laminate face-sheets and metal foam core studied by Zhang et al. (Zhang et al., 2018). Jing et al. (Jing et al., 2019) experimentally and numerically investigated response of the sandwich beams with aluminum alloy face-sheets and three core configurations includes positive layered-gradient core, negative layered-gradient core and non-gradient monolithic core.

In this research, the effect of graphene volume fraction on the response of methyl methacrylate cantilever beam under low velocity impact is investigated. The extended Halpin-Tsai model is used to determine the material properties of the beam. The nonlinear Hertz contact approach is applied to identify contact mechanism between impactor and beam surface. Using the first order shear deformation beam theory, the strains and stress are written. The equations of motion are driven with applying energy method, generalized Lagrange equations and Ritz method, and the equations solution is traced in time using the 4^{th} order Runge–Kutta approach.

2. Theoretical formulation

2.1 Extended Halpin-Tsai model

An isotropic polymer beam reinforced by aligned graphene sheets with length, width and thickness L, b and h is considered in this article, respectively (Fig. 1). The Cartesian coordinates system (x, y, z) is used in center of the beam that this beam is subjected to a spherical impactor with radius and mass R_i and M_i, and distance of the beam center X_i. The volume fractions of graphene and matrix phase are V^G and V^m, respectively, that are as:

$$V^G + V^m = 1 \tag{1}$$

The material properties of an isotropic polymer beam reinforced by aligned graphene sheets can be computed by Halpin-Tsai model (Affdl and Kardos, 1976):

$$E_{11} = \eta_1 E^m \frac{1 + 2\left(\frac{a_G}{h_G}\right)\gamma_{11}^G V^G}{1 - \gamma_{11}^G V^G}$$

$$E_{22} = \eta_2 E^m \frac{1 + 2\left(\frac{b_G}{h_G}\right)\gamma_{22}^G V^G}{1 - \gamma_{22}^G V^G}$$

$$G_{12} = \eta_3 G^m \frac{1}{1 - \gamma_{12}^G V^G}$$

$$\upsilon_{12} = V^G \upsilon_{12}^G + V^m \upsilon^m$$

$$\rho = V^G \rho^G + V^m \rho^m \tag{2}$$

Where η_1, η_2 and η_3 are the graphene efficiency parameters that can be estimated by comparing the results of MD simulations and Halpin-Tsai model (Shen et al., 2017). The parameters G and m shows graphene and matrix, the Young's modulus, shear modulus, density and Poisson ratio are E, G, ρ and v, the length, width and

effectivity thickness of graphene sheets are a_G, b_G and h_G, and the volume fraction is V. Parameters γ_{11}^G, γ_{22}^G and γ_{12}^G that can be used in Eq. (2) is as:

$$\gamma_{11}^G = \frac{\left(\frac{E_{11}^G}{E^m}\right) - 1}{\left(\frac{E_{11}^G}{E^m}\right) + 2\left(\frac{a_G}{h_G}\right)}$$

$$\gamma_{22}^G = \frac{\left(\frac{E_{22}^G}{E^m}\right) - 1}{\left(\frac{E_{22}^G}{E^m}\right) + 2\left(\frac{b_G}{h_G}\right)}$$

$$\gamma_{12}^G = \frac{\left(\frac{G_{12}^G}{G^m}\right) - 1}{\left(\frac{G_{12}^G}{G^m}\right)} \quad (3)$$

2.2 Contact model

The nonlinear Hertz contact model is used to specify the contact mechanism between the impactor and the beam F_i is as (Ranjbar and Feli, 2019a):

$$F_i = K_i\left(y - w_0(X_i,t)\right)^{\frac{3}{2}}$$

$$K_i = \frac{4}{3}\sqrt{R_i}\left(\frac{1}{E_{33,i}} + \frac{1-{\nu_i}^2}{E_i}\right)^{-1} \quad (4)$$

Where K_i is contact stiffness, y is impactor displacement and w_0 is beam displacement in the impact location X_i. Also, E_i and $E_{33,i}$ are Young's modulus of impactor and beam surface in the impact point and ν_i is Poisson's ratio of the impactor. Using MD simulations, Lin et al. (Lin et al., 2017) computed the transverse Young's modulus $E_{33,i}$ for graphene reinforced composites that is used in this article.

2.3 Energy method

The first order shear deformation beam theory (FSDT) is used to write the beam displacement field (Abrate, 2005):

$$u(x,y,z,t) = u_0(x,t) + z\varphi(x,t)$$
$$w(x,y,z,t) = w_0(x,t) \quad (5)$$

Where u_0, w_0 and φ are the displacement along x, z directions and rotation of the cross section of mid-plane. The stored strain energy (P) and kinetic energy (T) of the beam and impactor are as (Ranjbar and Feli, 2018):

$$P = \frac{1}{2}\int_{-L/2}^{L/2}\int_A (\sigma_{xx}\varepsilon_{xx} + K_s\sigma_{xz}\gamma_{xz})dAdx + \frac{2}{5}K_i(y - w_0(x_i,t))^{\frac{5}{2}}$$
$$T = \frac{1}{2}\int_{-L/2}^{L/2}\int_A \rho(\dot{u}^2 + \dot{w}^2)dAdx + \frac{1}{2}M_i\dot{y}^2 \quad (6)$$

Where K_s is shear correction factor, σ_{xx} and ε_{xx} are stress and strain along x direction and σ_{xz} and γ_{xz} are shear stress and shear strain in xz plane (Jones, 2014):

$$\varepsilon_{xx} = \frac{\partial u}{\partial x}$$

$$\gamma_{xz} = \frac{\partial u}{\partial z} + \frac{\partial w}{\partial x}$$

$$\sigma_{xx} = \overline{Q}_{11}\varepsilon_{xx}$$

$$\sigma_{xz} = K_s\overline{Q}_{55}\gamma_{xz} \quad (7)$$

Where $\overline{Q}_{11}$ and $\overline{Q}_{55}$ are the transformed reduced stiffness for each layer of the beam (Jones, 2014).

2.4 Ritz method

Using the Ritz method (Ansari et al., 2014):

$$u_0(x,t) = \sum_{n=1}^{N} U_n(t)N_n^u(x)$$

$$w_0(x,t) = \sum_{n=1}^{N} W_n(t)N_n^w(x)$$

$$\varphi_0(x,t) = \sum_{n=1}^{N} \Phi_n(t)N_n^\varphi(x) \quad (8)$$

Where $N_n^u(x)$, $N_n^w(x)$ and $N_n^\varphi(x)$ are the shape functions to apply geometric boundary conditions using the basic functions *Ls* and *Rs*. In this article the polynomial shape functions are applied (Lin and Xiang, 2014):

$$N_n^u(x) = x^{n-1} \times LS_u \times RS_u$$

$$N_n^w(x) = x^{n-1} \times LS_w \times RS_w$$

$$N_n^{\varphi}(x) = x^{n-1} \times LS_{\varphi} \times RS_{\varphi} \tag{9}$$

2.5 Matrix form of the equations of motion

Finally, using the generalized Lagrange equations (Greenwood, 2006), the matrix form of the equations of motion can be written as:

$$\begin{bmatrix} [M_{11}] & [M_{12}] & [M_{13}] \\ [M_{21}] & [M_{22}] & [M_{23}] \\ [M_{31}] & [M_{32}] & [M_{33}] \end{bmatrix} \begin{Bmatrix} \{\ddot{U}_n\} \\ \{\ddot{W}_n\} \\ \{\ddot{\Phi}_n\} \end{Bmatrix} + \begin{bmatrix} [K_{11}] & [K_{12}] & [K_{13}] \\ [K_{21}] & [K_{22}] & [K_{23}] \\ [K_{31}] & [K_{32}] & [K_{33}] \end{bmatrix} \begin{Bmatrix} \{U_n\} \\ \{W_n\} \\ \{\Phi_n\} \end{Bmatrix} = \begin{Bmatrix} 0 \\ F_i N_n^w(x_i) \\ 0 \end{Bmatrix}$$

$$M_i \ddot{y} = -F_i \tag{10}$$

Where *[M]* and *[K]* are mass matrix and stiffness matrix (Appendix) and Eq. (10) is a system of $3N + 1$ time-dependent coupled nonlinear equations with initial conditions:

$$U_n(0) = 0, \dot{U}_n(0) = 0$$

$$W_n(0) = 0, \dot{W}_n(0) = 0$$

$$\Phi_n(0) = 0, \dot{\Phi}_n(0) = 0$$

$$y(0) = 0, \dot{y}(0) = V_i \tag{11}$$

Where the impactor initial velocity is V_{imp}. In this article, in order to solve the equations of motion, the fourth-order Runge–Kutta method is used.

3. Validation

Because there is no research about polymer cantilever beam reinforced by aligned graphene sheets subjected to low velocity impact, the example of low velocity

impact on the FGM cantilever beam that is carried out by Kiani et al. (Kiani et al., 2013), is performed using present analytical method. This FGM beam is made of metal (Stainless-Steel) and ceramic (Silicon-Nitride) that are distributed along the thickness direction. The metal volume fraction is $V_m = 1 - V_c$ and ceramic volume fraction is $V_c = \left(\frac{1}{2} + \frac{z}{h}\right)^{\xi}$ and using the integrating method along the thickness direction are equal to $V_{m.t} = \frac{\xi}{1+\xi}$ and $V_{c.t} = \frac{1}{1+\xi}$, respectively. In this example, the value of ξ is equal to 1. The values $E_m = 201.04$ MPa, $\rho_m = 8166$ $\frac{\text{kg}}{\text{m}^3}$ and $\nu_m = 0.32622$ and $E_c = 348.43$ MPa, $\rho_c = 2370\frac{\text{kg}}{\text{m}^3}$ are used. The rigid spherical impactor with radius, mass and initial velocity 12.7 mm, 30 gr and 0.5 m/s impact on the center of the beam with length 153.5 mm, width 10 mm and thickness 10 mm. The contact force history between present analytical method and those are reported in Ref. (Kiani et al., 2013) is illustrated in Fig. 2. As seen from this Fig., the maximum contact force is 678 N using present analytical method and is 694 N form Ref. (Kiani et al., 2013) with 2.36% relative difference which indicates appropriate agreement.

4. Results and discussion

In this article, low velocity impact of steel spherical impactor with radius and initial velocity 12.7 mm and 0.5 m/s on the center of the cantilever beam with length 153.5 mm, width 10 mm and thickness 10 mm, are considered. The beam has 10 layers with stacking $(0/90/0/90/0)_s$ and is made of methyl methacrylate

(PMMA) reinforced by aligned single layer graphene sheets. The mechanical properties of PMMA at 300 K are E^m =2.5 GPa, ρ^m=1150 Kg/m^3 and υ^m=0.34. The aligned single layer graphene sheets at 300 K with specifications a_G=14.76 nm, b_G=14.77 nm, h_G= 0.188 nm, ν_{12}^G = 0.177, ρ^G =4118 kg/m^3, E_{11}^G= 1812 GPa, E_{22}^G =1870 GPa and G_{12}^G= 683 GPa, is used (Lin et al., 2017). The graphene efficiency parameters η_1, η_2 and η_3 and transverse Young's modulus $E_{33,i}$ for various volume fractions of graphene at 300 K are presented in Table 1. In this article, the value of shear moduli $G_{13} = G_{23} = 0.5G_{12}$, are considered.

Present section is performed to show the effect of the graphene volume fraction rise on the low velocity impact response of methyl methacrylate cantilever beam reinforced by aligned single layer graphene sheets. The contact force history of methyl methacrylate (PMMA) cantilever beam reinforced by aligned single layer graphene sheets for various volume fractions of graphene are illustrated in Fig. 3. This Fig. shows that the values of peak contact forces are 170.66 N, 181.98 N, 200.23 N and 216.86 N for graphene volume fractions 0.03, 0.05, 0.07 and 0.09, respectively, and the contact durations are 614.78 μs, 539.82 μs, 485.32 μs and 460.88 μs, respectively. These results indicate that the peak contact force is increased 6.63%, 10.03% and 8.3% and contact duration is decreased 12.19%, 10.1% and 5.04% with increasing graphene volume fraction from 0.03 to 0.05, 0.05 to 0.07 and 0.07 to 0.09, respectively. In order to examine the trend of results, it can be noted that transverse Young's modulus E_{33} is increased with increasing

graphene volume fraction in Table 1, also the contact stiffness in Eq. (4) increases with increasing $E_{33,i}$ and finally the contact force increases in Eq. (4) with increasing contact stiffness.

Time histories of shear strain and shear stress at the impact position are illustrated in Figs. 4 and5 at four graphene volume fractions V^G = 0.03, 0.05, 0.07 and 0.09. As seen from this Figs., an increase in graphene volume fraction, which result in higher shear strain and shear stress at peak contact force. The values of shear strain at peak contact force are about -7.402×10^{-6}, -11.736×10^{-6}, -13.335×10^{-6} and -12.234×10^{-6} corresponding to values graphene volume fractions 0.03, 0.05, 0.07 and 0.09, respectively, these values are about -0.0347 MPa, -0.0756 MPa, -0.1297 MPa and -0.1692 MPa for shear stress at peak contact force, respectively. Results show that shear strain and shear stress at peak contact force have an increase of about 58.55% and 117.87% as the graphene volume fraction increases from 0.03 to 0.05, respectively, while there is about 13.62% and 71.56% as the graphene volume fraction increases from 0.05 to 0.07, respectively, and there is about 8.26% and 30.45% as the graphene volume fraction increases from 0.07 to 0.09, respectively.

By reviewing the article data one can come to this goal that the trend of peak contact force, shear strain and shear stress at peak contact force are the same and increase for increasing graphene volume fraction while the impact duration tends vice versa. The effect of increasing of graphene volume fraction from 0.03 to 0.05 on responses are greater than on graphene volume fraction increasing from 0.05

to 0.07, and increasing of graphene volume fraction from 0.07 to 0.09 has the least effect on response changes. Also, the most influence of increasing of the graphene volume fraction is for changing of shear stress at the peak contact force.

5. Conclusions

In this article, the effect of graphene volume fraction increasing on the response of low velocity impact on the methyl methacrylate cantilever beam reinforced by aligned single layer graphene sheets are investigated. The specific observations of this article are:

- There is a good match between this analytical approach and another paper data.
- With increasing graphene volume fractions, the peak contact force, shear strain and shear stress at peak contact force are enhanced and contact time is decreased.
- The most changes in responses is maximum for changing of graphene volume fraction from 0.03 to 0.05, followed by 0.05 to 0.07 an 0.07 to 0.09.
- Among the peak contact force, contact time, shear strain and shear stress at the peak contact force, the shear stress at the peak contact force has the most changing with graphene volume fraction increasing.

Appendix

The mass matrix arrays are as:

$$M_{11}^{mn} = \int_{-\frac{h}{2}}^{+\frac{h}{2}} \int_{-\frac{L}{2}}^{+\frac{L}{2}} b\rho N_m^u N_n^u dxdz$$

$$M_{12}^{mn} = 0$$

$$M_{13}^{mn} = \int_{-\frac{h}{2}}^{+\frac{h}{2}} \int_{-\frac{L}{2}}^{+\frac{L}{2}} b\rho z N_m^u N_n^\varphi dxdz$$

$$M_{21}^{mn} = 0$$

$$M_{22}^{mn} = \int_{-\frac{h}{2}}^{+\frac{h}{2}} \int_{-\frac{L}{2}}^{+\frac{L}{2}} b\rho N_m^w N_n^w dxdz$$

$$M_{23}^{mn} = 0$$

$$M_{31}^{mn} = \int_{-\frac{h}{2}}^{+\frac{h}{2}} \int_{-\frac{L}{2}}^{+\frac{L}{2}} b\rho z N_m^\varphi N_n^u dxdz$$

$$M_{32}^{mn} = 0$$

$$M_{33}^{mn} = \int_{-\frac{h}{2}}^{+\frac{h}{2}} \int_{-\frac{L}{2}}^{+\frac{L}{2}} b\rho z^2 N_m^\varphi N_n^\varphi dxdz$$

The stiffness matrix arrays are as:

$$K_{11}^{mn} = \int_{-\frac{h}{2}}^{+\frac{h}{2}} \int_{-\frac{L}{2}}^{+\frac{L}{2}} b\overline{Q}_{11} \frac{dN_m^u dN_n^u}{dx \quad dx} dxdz$$

$$K_{12}^{mn} = 0$$

$$K_{13}^{mn} = \int_{-\frac{h}{2}}^{+\frac{h}{2}} \int_{-\frac{L}{2}}^{+\frac{L}{2}} b\overline{Q}_{11} z \frac{dN_m^u dN_n^\varphi}{dx \quad dx} dxdz$$

$$K_{21}^{mn} = 0$$

$$K_{22}^{mn} = \int_{-\frac{h}{2}}^{+\frac{h}{2}} \int_{-\frac{L}{2}}^{+\frac{L}{2}} b\bar{Q}_{55} \frac{dN_m^w dN_n^w}{dx \quad dx} dxdz$$

$$K_{23}^{mn} = \int_{-\frac{h}{2}}^{+\frac{h}{2}} \int_{-\frac{L}{2}}^{+\frac{L}{2}} b\bar{Q}_{55} \frac{dN_m^w}{dx} N_{\ n}^{\varphi} dxdz$$

$$K_{31}^{mn} = \int_{-\frac{h}{2}}^{+\frac{h}{2}} \int_{-\frac{L}{2}}^{+\frac{L}{2}} b\bar{Q}_{11} z \frac{dN_m^{\varphi} dN_n^u}{dx \quad dx} dxdz$$

$$K_{32}^{mn} = \int_{-\frac{h}{2}}^{+\frac{h}{2}} \int_{-\frac{L}{2}}^{+\frac{L}{2}} b\bar{Q}_{55} N_n^{\varphi} \frac{dN_n^w}{dx} dxdz$$

$$K_{33}^{mn} = \int_{-\frac{h}{2}}^{+\frac{h}{2}} \int_{-\frac{L}{2}}^{+\frac{L}{2}} b\bar{Q}_{11} z^2 \frac{dN_m^{\varphi} dN_n^{\varphi}}{dx \quad dx} dxdz + \int_{-\frac{h}{2}}^{+\frac{h}{2}} \int_{-\frac{L}{2}}^{+\frac{L}{2}} b\bar{Q}_{55} N_m^{\varphi} N_n^{\varphi} dxdz$$

Refecences

ABRATE, S. 2005. *Impact on composite structures*, Cambridge university press.

AFFDL, J. H. & KARDOS, J. 1976. The Halpin - Tsai equations: a review. *Polymer Engineering & Science,* 16**,** 344-352.

ANSARI, R., SHOJAEI, M. F., MOHAMMADI, V., GHOLAMI, R. & SADEGHI, F. 2014. Nonlinear forced vibration analysis of functionally graded carbon nanotube-reinforced composite Timoshenko beams. *Composite Structures,* 113**,** 316-327.

GREENWOOD, D. T. 2006. *Advanced dynamics*, Cambridge University Press.

HEYDARI-MEYBODI, M., SABER-SAMANDARI, S. & SADIGHI, M. 2016. An experimental study on low-velocity impact response of nanocomposite beams reinforced with nanoclay. *Composites Science and Technology,* 133**,** 70-78.

HUANG, X., QI, X., BOEY, F. & ZHANG, H. 2012. Graphene-based composites. *Chemical Society Reviews,* 41**,** 666-686.

JAM, J. & KIANI, Y. 2015. Low velocity impact response of functionally graded carbon nanotube reinforced composite beams in thermal environment. *Composite Structures,* 132**,** 35-43.

JING, L., SU, X., CHEN, D., YANG, F. & ZHAO, L. 2019. Experimental and numerical study of sandwich beams with layered-gradient foam cores under low-velocity impact. *Thin-Walled Structures,* 135**,** 227-244.

JONES, R. M. 2014. *Mechanics of composite materials*, CRC press.

KIANI, Y., SADIGHI, M., SALAMI, S. J. & ESLAMI, M. 2013. Low velocity impact response of thick FGM beams with general boundary conditions in thermal field. *Composite Structures,* 104**,** 293-303.

LI, D. & KANER, R. B. 2008. Graphene-based materials. *Science,* 320**,** 1170-1171.

LIN, F. & XIANG, Y. 2014. Vibration of carbon nanotube reinforced composite beams based on the first and third order beam theories. *Applied Mathematical Modelling,* 38**,** 3741-3754.

LIN, F., XIANG, Y. & SHEN, H.-S. 2017. Temperature dependent mechanical properties of graphene reinforced polymer nanocomposites–a molecular dynamics simulation. *Composites Part B: Engineering,* 111**,** 261-269.

QIN, Q., XIANG, C., ZHANG, J., WANG, M., WANG, T. & POH, L. 2017. On low-velocity impact response of metal foam core sandwich beam: a dual beam model. *Composite Structures,* 176**,** 1039-1049.

RANJBAR, M. & FELI, S. 2018. Low velocity impact analysis of an axially functionally graded carbon nanotube reinforced cantilever beam. *Polymer Composites,* 39**,** E969-E983.

RANJBAR, M. & FELI, S. 2019a. Mechanical and low-velocity impact properties of epoxy-composite beams reinforced by MWCNTs. *Journal of Composite Materials,* 53**,** 693-705.

RANJBAR, M. & FELI, S. 2019b. Temperature-dependent analysis of axially functionally graded CNT reinforced micro-cantilever beams subjected to low velocity impact. *Mechanics of Advanced Materials and Structures,* 26**,** 1154-1168.

SALAMI, S. J. 2017. Low velocity impact response of sandwich beams with soft cores and carbon nanotube reinforced face sheets based on extended high order sandwich panel theory. *Aerospace Science and Technology,* 66**,** 165-176.

SHEN, H.-S., LIN, F. & XIANG, Y. 2017. Nonlinear vibration of functionally graded graphene-reinforced composite laminated beams resting on elastic foundations in thermal environments. *Nonlinear Dynamics,* 90**,** 899-914.

ZHANG, J., YE, Y., QIN, Q. & WANG, T. 2018. Low-velocity impact of sandwich beams with fibre-metal laminate face-sheets. *Composites Science and Technology,* 168**,** 152-159.

Table 1. The graphene efficiency parameters η_1, η_2 and η_3 and transverse Young's modulus E_{33} for various volume fractions of graphene V^G at 300 K (Lin et al., 2017).

V^G	η_1	η_2	η_3	$E_{33,i}$ (GPa)
0.03	2.929	2.855	11.842	3.401
0.05	3.068	2.962	15.944	3.663
0.07	3.013	2.966	23.575	4.380
0.09	2.647	2.609	32.816	5.182

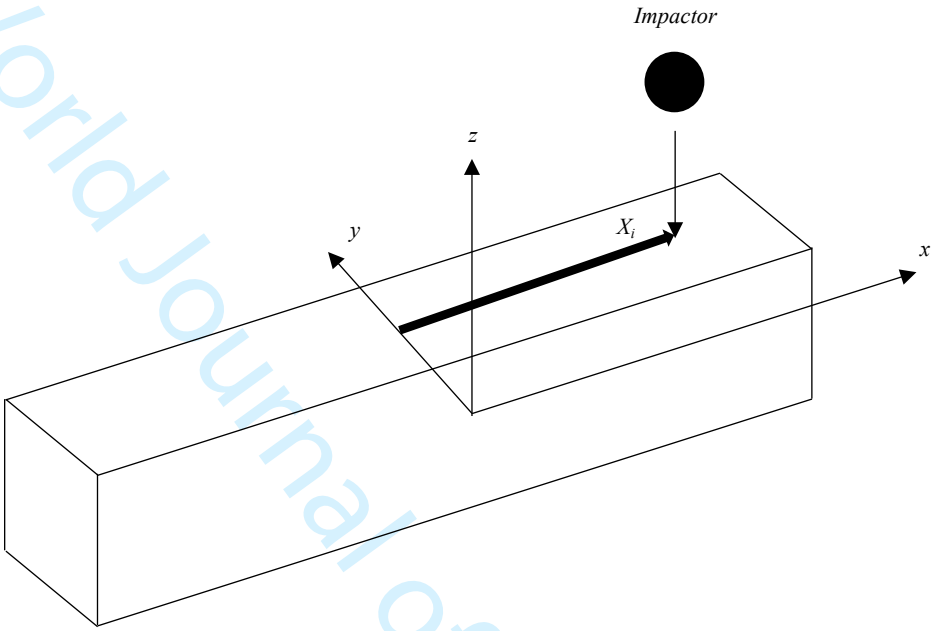

Fig. 1. Schematic of low velocity impact on the isotropic polymer beam reinforced by aligned graphene sheets.

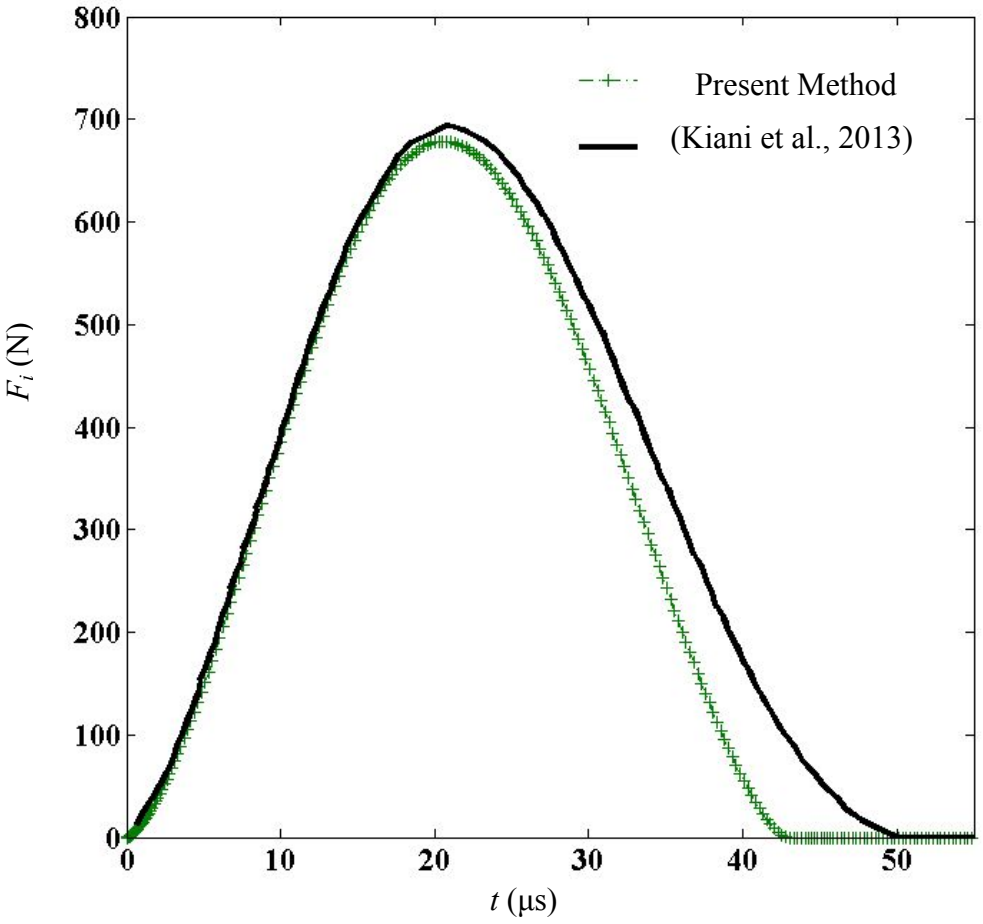

Fig. 2. Comparison of contact force history between present method and Kiani et al. model for low velocity impact on the FGM cantilever beam.

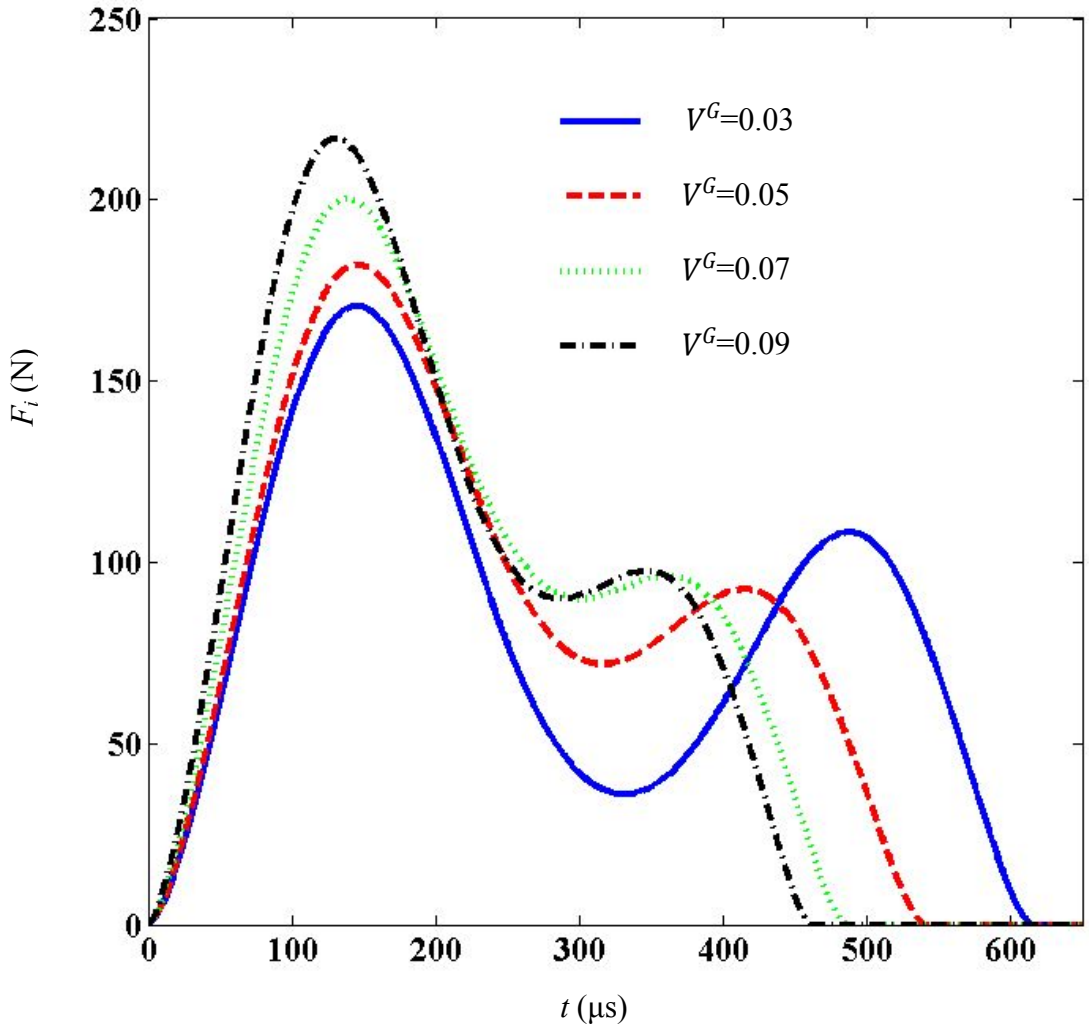

Fig. 3. The contact force history of methyl methacrylate (PMMA) cantilever beam reinforced by aligned single layer graphene sheets for various volume fractions of graphene.

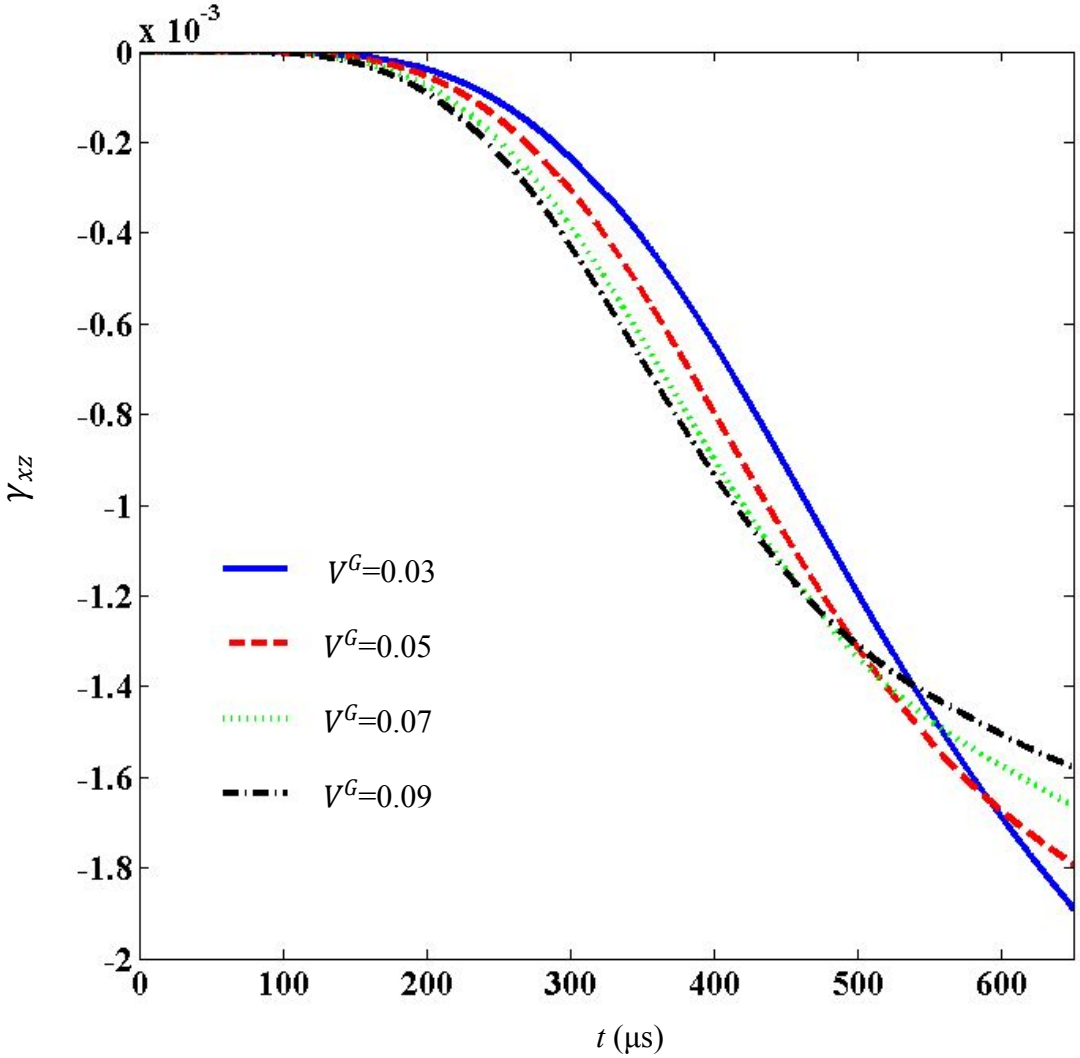

Fig. 4. The shear strain history at the beam impact point, of methyl methacrylate (PMMA) cantilever beam reinforced by aligned single layer graphene sheets for various volume fractions of graphene.

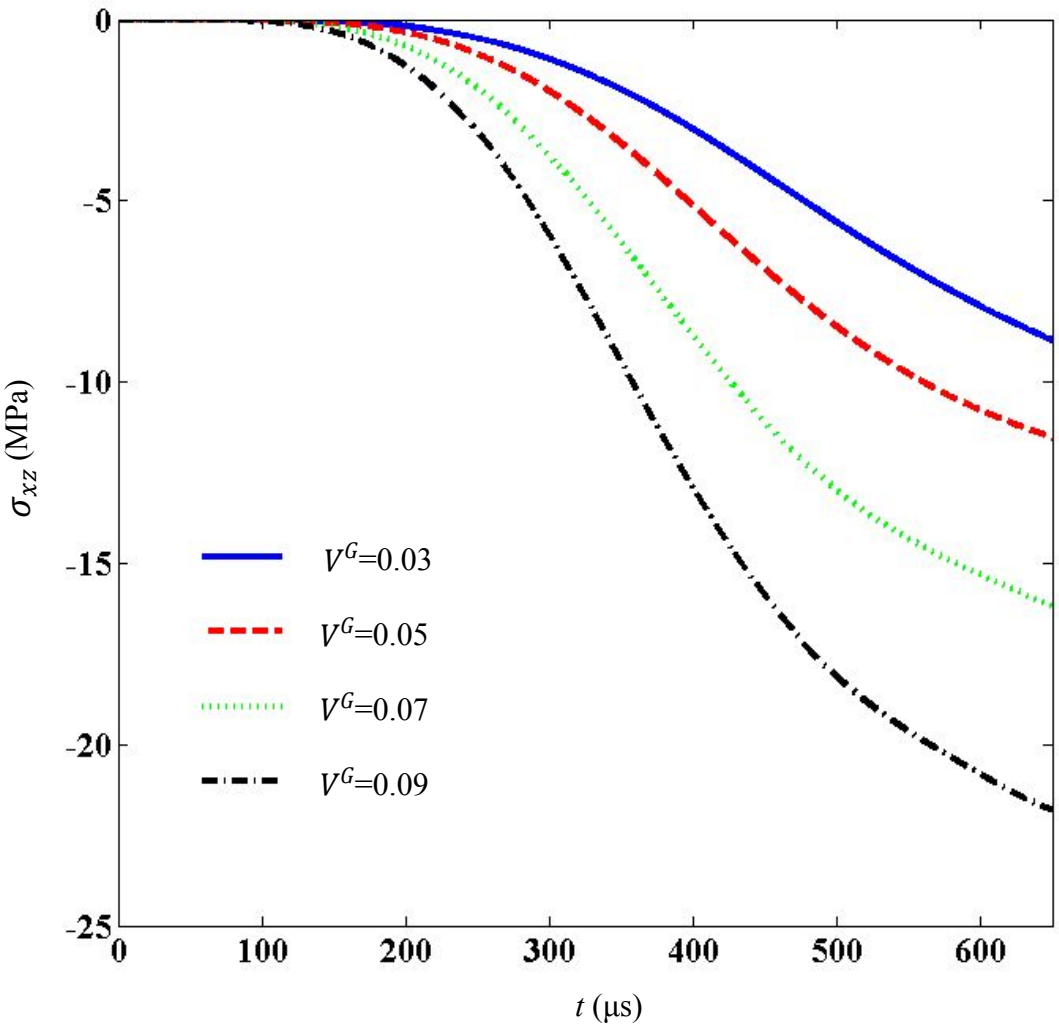

Fig. 5. The shear stress history at beam impact point, of methyl methacrylate (PMMA) cantilever beam reinforced by aligned single layer graphene sheets for various volume fractions of graphene.